#### **OPEN ACCESS**



# Evidence of Jet Activity from the Secondary Black Hole in the OJ 287 Binary System

```
Mauri J. Valtonen<sup>1,2</sup>, Staszek Zola<sup>3</sup>, Alok C. Gupta<sup>4,5</sup>, Shubham Kishore<sup>4</sup>, Achamveedu Gopakumar<sup>6</sup>
         Svetlana G. Jorstad<sup>7</sup>, Paul J. Wiita<sup>8</sup>, Minfeng Gu<sup>5</sup>, Kari Nilsson<sup>1</sup>, Alan P. Marscher<sup>7</sup>, Zhongli Zhang<sup>9,10</sup>,
Rene Hudec 11,12, Katsura Matsumoto 13, Marek Drozdz 14, Waldemar Ogloza 14, Andrei V. Berdyugin 2, Daniel E. Reichart 15, Daniel E. Reic
         Markus Mugrauer<sup>16</sup>, Lankeswar Dey<sup>17</sup>, Tapio Pursimo<sup>18</sup>, Harry J. Lehto<sup>2</sup>, Stefano Ciprini<sup>19,20</sup>, T. Nakaoka<sup>21</sup>,
              M. Uemura<sup>21</sup>, Ryo Imazawa<sup>22</sup>, Michal Zejmo<sup>23</sup>, Vladimir V. Kouprianov<sup>15</sup>, James W. Davidson, Jr.<sup>24</sup>, Alberto Sadun<sup>25</sup>, Jan Štrobl<sup>12</sup>, Z. R. Weaver<sup>7</sup>, and Martin Jelínek<sup>12</sup>, FINCA, University of Turku, FI-20014 Turku, Finland
                                           <sup>2</sup> Tuorla Observatory, Department of Physics and Astronomy, University of Turku, FI-20014 Turku, Finland
                                         Astronomical Observatory, Jagiellonian University, ul. Orla 171, 30-244 Krakow, Poland; szola@oa.uj.edu.pl
                                                Aryabhatta Research Institute of Observational Sciences (ARIES), Manora Peak, Nainital-263001, India
<sup>5</sup> Key Laboratory for Research in Galaxies and Cosmology, Shanghai Astronomical Observatory, Chinese Academy of Sciences, 80 Nandan Road, Shanghai 200030,
                                                                                                            People's Republic of China
                                         <sup>6</sup> Department of Astronomy and Astrophysics, Tata Institute of Fundamental Research, Mumbai 400005, India
                                        Institute for Astrophysical Research, Boston University, 725 Commonwealth Avenue, Boston, MA 02215, USA
                                            Department of Physics, The College of New Jersey, 2000 Pennington Road, Ewing, NJ 08628-0718, USA
                                     Shanghai Astronomical Observatory, Chinese Academy of Sciences, Shanghai 200030, People's Republic of China
10 Key Laboratory of Radio Astronomy and Technology, Chinese Academy of Sciences, A20 Datun Road, Chaoyang District, Beijing 100101, People's Republic of China
                                    Faculty of Electrical Engineering, Czech Technical University, 166 36 Prague, Czech Republic; rene.hudec@gmail.com
                                                                            Astronomical Institute (ASU CAS), 251 65 Ondřejov, Czech Republic
                  13 Astronomical Institute, Osaka Kyoiku University, 4-698 Asahigaoka, Kashiwara, Osaka 582-8582, Japan; katsura@cc.osaka-kyoiku.ac.jp

14 Mt. Suhora Astronomical Observatory, University of the National Education Commission, ul.Podchorazych 2, 30-084 Krakow, Poland
               Department of Physics and Astronomy, University of North Carolina at Chapel Hill, Chapel Hill, NC 27599, USA; dan.reichart@gmail.com,
                                                                                                              v.kouprianov@gmail.com
                             Astrophysical Institute and University Observatory, Schillergässchen 2, D-07745 Jena, Germany; markus@astro.uni-jena.de
                         17 Department of Physics and Astronomy, West Virginia University, P.O. Box 135, Willey Street, Morgantown, WV 26506, USA

18 Nordic Optical Telescope, Apartado 474, E-38700 Santa Cruz de La Palma, Spain; tpursimo@not.iac.es
                                                           Istituto Nazionale di Fisica Nucleare, Sezione di Roma "Tor Vergata", I-00133 Roma, Italy
                        <sup>20</sup> Space Science Data Center—Agenzia Spaziale Italiana, Via del Politecnico, snc, I-00133, Roma, Italy; stefano.ciprini@ssdc.asi.it
                      <sup>21</sup> Hiroshima Astrophysical Science Center, Hiroshima University, 1-3-1 Kagamiyama, Higashi-Hiroshima, Hiroshima 739-8526, Japan
Department of Physics, Graduate School of Advanced Science and Engineering, Hiroshima University, 1-3-1 Kagamiyama, Higashi-Hiroshima, Hiroshima 739-8526, Japan
                              Kepler Institute of Astronomy, University of Zielona Gora, Lubuska 2, 65-265 Zielona Gora, Poland; michalzejmo@gmail.com
                        24 Department of Astronomy, University of Virginia, 530 McCormick Road, Charlottesville, VA 22904, USA; jimmy@virginia.edu
                                                 Department of Physics, University of Colorado, Denver, CO 80217, USA; alberto.sadun@ucdenver.edu
                                                    Received 2024 April 11; revised 2024 April 27; accepted 2024 April 29; published 2024 June 11
```

#### **Abstract**

We report the study of a huge optical intraday flare on 2021 November 12 at 2 a.m. UT in the blazar OJ 287. In the binary black hole model, it is associated with an impact of the secondary black hole on the accretion disk of the primary. Our multifrequency observing campaign was set up to search for such a signature of the impact based on a prediction made 8 yr earlier. The first *I*-band results of the flare have already been reported by Kishore et al. (2024). Here we combine these data with our monitoring in the *R*-band. There is a big change in the *R*-*I* spectral index by  $1.0 \pm 0.1$  between the normal background and the flare, suggesting a new component of radiation. The polarization variation during the rise of the flare suggests the same. The limits on the source size place it most reasonably in the jet of the secondary BH. We then ask why we have not seen this phenomenon before. We show that OJ 287 was never before observed with sufficient sensitivity on the night when the flare should have happened according to the binary model. We also study the probability that this flare is just an oversized example of intraday variability using the Krakow data set of intense monitoring between 2015 and 2023. We find that the occurrence of a flare of this size and rapidity is unlikely. In machine-readable Tables 1 and 2, we give the full orbit-linked historical light curve of OJ 287 as well as the dense monitoring sample of Krakow.

Unified Astronomy Thesaurus concepts: High energy astrophysics (739) Supporting material: machine-readable tables

# 1. Introduction

OJ 287 is a highly variable BL Lacertae-type quasar at a rather low redshift of 0.306 (Sitko & Junkkarinen 1985). It is

Original content from this work may be used under the terms of the Creative Commons Attribution 4.0 licence. Any further distribution of this work must maintain attribution to the author(s) and the title of the work, journal citation and DOI.

easily observable even with small telescopes. Because it lies close to the ecliptic, it has been accidentally photographed since 1887 during searches of minor planets and other objects near the ecliptic plane. This has produced a vast amount of data: several hundred photometric measurements and interesting upper limits prior to 1970. The magnitude data display an easily discernible 12 yr cycle, modified by another 55 yr cycle. These come out prominently in quantitative analysis but are easily seen by just looking at the light curve (Figure 1). In

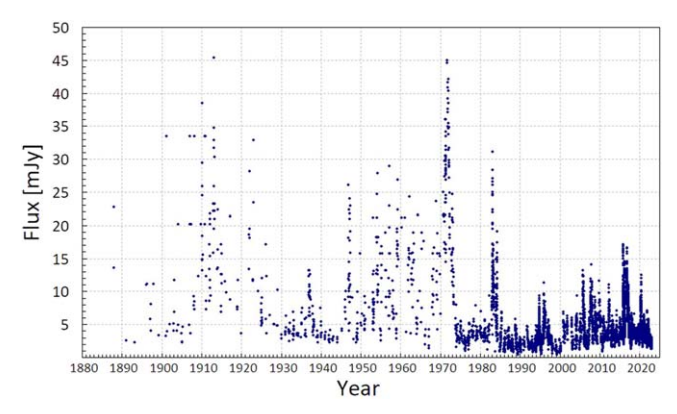


Figure 1. V-band historical light curve of OJ 287.

addition, the dense network of upper limits puts severe restrictions on the light curve in the parts where the photometric data are sparse (e.g., Valtonen et al. 2021, 2023c, and references therein).

The understanding of the two light-curve cycles as well as the exact times of the large flares is paramount to any theoretical model. The large flares typically represent a 2 mag rise in brightness. In addition to the flares seen in the photometric data, there are only a very limited number of flares that can exist without violating the upper limit network. A mathematical sequence, called Keplerian sequence, similar in nature to the Balmer formula for the hydrogen spectral lines, gives all the observed flares seen in OJ 287 and does not contradict the upper limits of the photometry of OJ 287 (Valtonen et al. 2023c). There are currently 26 members in this sequence from 1886 to the present. The sequence is based on a simple analytical model of binary motion.

The sequence provides a way of predicting future flares with an accuracy of about 1 yr. All it requires is the assumption that the system consists of an unequal-mass binary black hole (BH) pair and a gas disk. The signals arise from the plunging of the secondary BH through the gas disk.

An even simpler method is to take a stretch of the old light curve of OJ 287 and slide it forward on the time axis to future time. It does not necessarily need any astrophysical theory to back it up. It is a purely phenomenological method, and all it requires is that there is some sort of repeatability in the system. This method has been used to justify observing campaigns during specified periods of time. The past experience is that the sliding-on-the-time-axis method is useful with about 1 yr accuracy; i.e., it can be used to justify the starting of observing campaigns over a specific observing season independent of any astrophysical theory.

Then there are highly accurate models that predict the times of the flares with an accuracy of up to 4 hr (Laine et al. 2020). The following values for OJ 287's BH binary system are found: primary mass  $m_1 = 18.35 \pm 0.05 \times 10^9~M_{\odot}$ , secondary mass  $m_2 = 150 \pm 10 \times 10^6~M_{\odot}$ , primary Kerr parameter  $\chi_1 = 0.38 \pm 0.05$ , orbital eccentricity  $e = 0.657 \pm 0.003$ , and orbital period (redshifted)  $P = 12.06 \pm 0.01$  yr.

The Keplerian sequence is just an example of approximate solutions to the timings of the flares. The full solution was calculated by using a binary BH model in general relativity up to post-Newtonian order 4.5, spin—orbit interaction, a standard accretion disk of two parameters, and accurate calculations of disk bending. Also, the feedback of the disk potential onto the binary orbit was included in a self-consistent way, even though

it was found to be insignificant (Sillanpaa et al. 1988; Sundelius et al. 1997). The direction of the observer relative to the disk was also taken into account (Iyanov et al. 1998).

The total number of parameters is eight. The method solves the parameters by a convergent method similar to the Newton–Raphson method. The method requires the exact timings of nine flares and solves the correct times for another eight flares that have been sufficiently observed. In addition, it satisfies strict observational constraints in many cases where a flare was not seen, but the region of the light curve is densely covered by upper limits. Even though the convergent method is efficient, it still requires millions of orbit solutions to find out the range of uncertainties of the parameters, in addition to their most likely values.

All the free parameters are related to the astrophysical model. The theory of gravity and its numerical treatment are given and contain no parameters. In this way, the method differs from Zwick & Mayer (2023), who treat the theory of gravity by a parametric method and determine the parameters by fitting to OJ 287 observations. Then it remains unclear how the method differs from the standard gravitational theory.

In principle, the solution could fall on a false minimum rather than on the global minimum, as suggested by Zwick & Mayer (2023). However, if we look at the history of development of this model from 1995 to 2018, we see that the primary properties of the model (binary masses, orbital eccentricity, etc.) have not changed when greater astrophysical details have been included and the number of free parameters has increased from four to eight. The purely mathematical Keplerian sequence, with no astrophysical details beyond Newton's law of gravity and Einstein's explanation of the firstorder orbit precession, leads to the same orbit solution. The simplified model suggested by Zwick & Mayer (2023), even though lacking essential astrophysical details such as disk bending, direct calculation of disk potential by full N-body simulation, spin-orbit interaction, details of radiation processes, etc., leads to essentially the same solution of the main properties of the system as in the full solution.

The model was completed in 1995 and was presented in several papers thereafter. We call it the *standard model* in the following. It combines three accurate codes: the code of orbit calculation (Mikkola 2020), the code of disk potential calculation (Miller 1976), and the code of evolution of an expanding gas cloud, developed by Harry Lehto (Lehto & Valtonen 1996). These codes were combined into a single code by Björn Sundelius for application to the OJ 287 problem (Sundelius et al. 1997). This code also had a feature of either keeping the self-interaction inside the disk or removing it when it was not necessary in order to speed up the calculations. We should note that very similar codes are widely used in solving solar system problems where their functioning can be directly verified by observations (Salo 2012).

With the later addition of disk sidedness (that is, from which side we view the disk), spin-orbit interaction, disk bending, and the general relativistic tail terms, we may say that the full solution of the OJ 287 problem is currently comparable in accuracy to studies in the solar system. For example, we are able to predict the times of new flares in OJ 287 with the same relative accuracy as the next apparition of Halley's comet in the inner solar system.

The omission of the spin-orbit interaction and the disk bending both lead to errors in excess of 0.5 yr in the times of flares (Valtonen 2007; Valtonen et al. 2011). Thus, such models are of little interest today, besides proving that the full mathematical solution of the OJ 287 problem is unique.

The full solution was tested in 2019, when the observed flare came within 4 hr of the predicted time (Laine et al. 2020), and again in 2022, when the observations put strict limits on the timing even though the flare itself was not observable (Dey et al. 2018; Valtonen et al. 2023c).

The graphical sliding-on-the-time-axis approach was most recently used for the 2021–2022 multifrequency campaign. The usefulness of this method is that it does not use any specific model but gives an idea when to carry out observations on general grounds. These ideas were communicated in one paper (Valtonen et al. 2021) and in various prepublication notes (dated 2022 June, September, and November). In the final publication, it was shown that one must use multicolor data for the sliding to get useful results (Valtonen et al. 2023c). The prediction in the standard model was given in Dey et al. (2018). Using the *R*-band data alone produces a flare date that was far too late with respect to the accurate model, while the *B*-band data give excellent agreement.

The light-curve comparison between 2005 and 2022 also produced an important piece of additional information that we did not have before. The disk-crossing times require the knowledge of the disk level, i.e., how much the disk is bent above or below its mean level at the time and at the position of the disk crossing. Also, the astrophysical delay from the disk crossing to the observed flare has to be calculated. In principle, there could be errors in both quantities that accidentally cancel each without affecting the observed flare time. Valtonen et al. (2023c) showed that the astrophysical time delay can be directly measured in the 2005 disk impact, and the measurement agrees with the standard model within the errors.

The disk level calculation uses only low-level general relativistic corrections to the Newtonian theory. The corrections are quite standard; higher-level corrections are required for the binary motion but not for the disk motion, since we are not looking at the central parts of the disk. Comparing the simulations of the disk level between 2005 and 2022 disk impacts, it was found that the uncertainty is about 5 au (Valtonen et al. 2023b). In terms of travel time, this corresponds to about 12 hr at these impact distances. For disk impacts at a closer distance from the central BH (i.e., closer than 10,000 au), the mean level is zero, and the standard error of the mean is about 4 au (Valtonen 2007). The orbital speed at the pericenter is also higher than in the apocenter part of the orbit; therefore, the disk level uncertainty is below 4 hr in the timing of the pericenter flares. This is better than what can be determined from observations, which means that the disk level uncertainties play no role in the standard model.

However, it is important to differentiate between the full mathematical solution, which we call the *standard model*, and the graphical method. The reason why the graphical method works only with the *B*-band data is that the effects of the disk impact show primarily in the blue color, while the *R*-band data are dominated by the primary jet. The two types of activity take place in different regions of the system and cannot be simply connected (Valtonen et al. 2023b).

The observation of the main flare in 2022 was known to be impossible by ground-based optical telescopes. Radio observations were carried out, and they excluded the possibility that the observed flare sequence arises from activity in the primary jet.

If it did, we would have seen a radio flare in the summer of 2022, but there was no evidence of it.

However, there is another way to get essentially the same information from the optical light curve. In the model of Pihajoki et al. (2013b), it has been argued that the secondary BH becomes active at certain phases of the binary orbit, and these active stages can be used as orbit markers. If seen at the predicted times, this activity of the secondary component also confirms the orbit model.

The standard flares are interpreted as a result of the impacts of the secondary on the accretion disk. This causes thermal radiation from bubbles of gas that are pulled out of the disk. In contrast, the flares from the secondary itself would be associated with the jet of the secondary BH. This emission would appear on top of the normal emission from the primary jet during brief periods of time when the Roche lobe of the secondary is flooded by the disk gas. Even though the secondary is 122 times smaller in mass than the primary, during these special episodes, the emission of the secondary jet can overpower the emission of the primary jet and show up as large-amplitude intraday variability (IDV).

This Letter reports very dense photometry of OJ 287 during the period when the exact orbit solution makes us expect the jet emission from the secondary BH. It is complemented by polarimetric observations, which are less dense but can also provide useful information. We then compare our data with Kishore et al. (2024), who confirmed the appearance of the flare that we had already tentatively reported (Valtonen et al. 2023a). We then discuss our findings with respect to the theoretical model calculated by Pihajoki et al. (2013b). Finally, we use the model orbit file from 1887 onward, compare it with the available photometry of OJ 287, and ask whether the secondary BH flares have been seen previously at corresponding times. The significance of our findings is discussed in the conclusions.

#### 2. Data Collection and Reduction in the R-Band

For the flares that we usually discuss in OJ 287, the full width at half-maximum (FWHM) is from a few days to weeks (Valtonen et al. 2008). The question we pose here is whether even faster IDV flares exist. Until this campaign, none had been reported in OJ 287 in the same brightness category as the ordinary big flares ( $\geq$ 4 mJy in the *R*-band; Lehto & Valtonen 1996). But it does not mean that they do not exist. The shorter the flare timescale, the harder it is to catch them. And since we have a 12 yr periodicity, it is easy to see how a one-night event per 12 yr could be missed. It becomes crucial that there is already a reliable model that tells us when to organize a campaign.

The first attempt for such a campaign took place in 2013, with the inspiration of Pihajoki et al. (2013b). The Krakow monitoring program was active but not dense enough. The next chance came at the end of 2021, and this time we were better prepared, as we will now describe.

Photometric monitoring of OJ 287 within the Krakow Quasar Monitoring Program started in 2006. Initially, we performed observations at two Polish sites: Mt. Suhora Observatory of the Pedagogical University in Krakow and the Astronomical Observatory of the Jagiellonian University. Observations taken at the two nearby sites suffered gaps in data, mainly due to bad weather. Therefore, in 2013, the monitoring program started to use the prompt5 telescope,

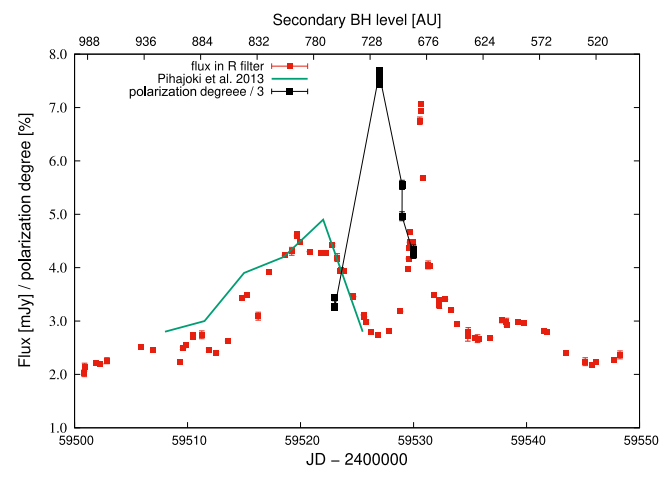


**Figure 2.** The *R*-band data (red squares), degree of polarization measurements (black squares), and a theoretical line from Pihajoki et al. (2013b). The time in Julian Days is given below, and the corresponding positions of the secondary BH above the disk are labeled on the top.

located in Chile and controlled by the Skynet Robotic Telescope Network (Zola et al. 2021). Since 2015, we have used seven optical telescopes within the Skynet Network. Due to their location on four continents and the telescope redundancy, we could gather data daily. Additional observations are being provided routinely by the Osaka Astronomical Observatory and the University Observatory Jena. During multisite campaigns, several other sites, located all over the globe, contributed photometric data that have previously been reported (Valtonen et al. 2023c and references therein). Images were reduced in a standard way: calibration of raw images was done using the IRAF package, while differential magnitudes were extracted with the CMunipack program, which is an interface to the DAOPHOT code. The data taken by the Skynet telescopes have been calibrated by the network pipeline. We used stars #4 and #10 (Fiorucci & Tosti 1996) as comparison and check stars, respectively. The photometric data reported and analyzed in this Letter cover the period between 2021 October 21 and December 1, when a huge flare in the optical band occurred. The data taken in the wideband R filter within this period consist of 562 single points binned into 42 mean ones with a 1 day bin. We adopted the brightness of the comparison star in the R filter as 13.74 mag (Fiorucci & Tosti 1996) and converted magnitudes into flux in mJy units. These data are shown in Figure 2 by red squares.

Altogether, until 2023 July 24, we gathered 63,480 individual points, which were binned with 12 hr bins, resulting in 3388 mean points. We make the data available in Table 1. Due to its length, we show here only the first 10 entries. Individual data are also available on request.

# 3. Comparison between TESS *I*-band and Our *R*-band Observations

At the end of 2021, during the period of 80 days, the Transiting Exoplanet Survey Satellite (TESS) observed OJ 287 almost continuously. This is the period of time when, according to prior estimates, the secondary should have approached the primary disk from our side and triggered the secondary jet activity (Pihajoki et al. 2013b; Valtonen et al. 2021). Figure 3 illustrates the situation.

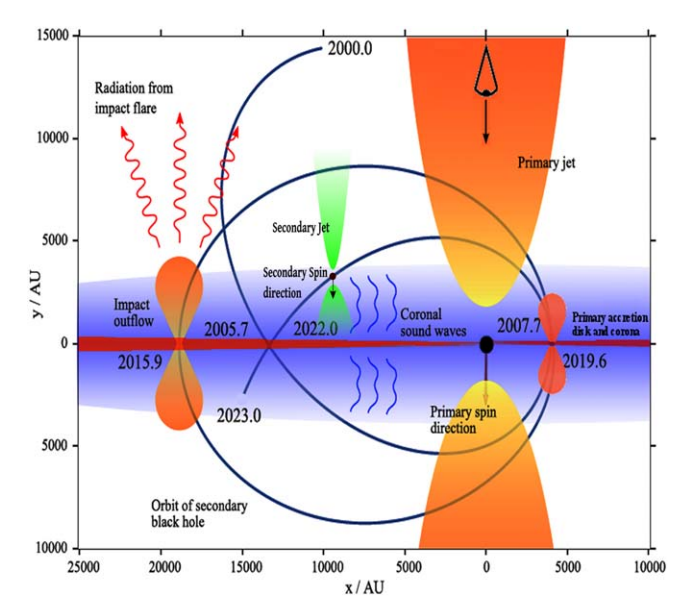


**Figure 3.** The binary model of OJ 287. The secondary jet pointing at us is thought to be the source of the 2021 November 12 flare. The size of the radiating region is comparable to the expected cross section of this jet but far too small for the cross section of the primary jet.

Table 1
OJ 287 Mean Points Gathered in the *R* Filter during the Period between 2006
September 30 and 2023 June 24

$\overline{\mathrm{JD}_{\mathrm{hel}}}$	OJ 287-comp (mag)	σ	NPTS
2454008.598390	1.557	0.003	40
2454039.645830	1.204	0.005	21
2454047.617653	1.821	0.005	37
2454073.528083	1.357	0.007	9
2454075.480830	1.368	0.030	3
2454075.647513	1.375	0.004	14
2454081.462389	1.611	0.004	11
2454081.517999	1.622	0.003	13
2454084.450372	1.575	0.002	16
2454084.534483	1.581	0.007	6

**Note.** For the brightness of the comparison star, see Fiorucci & Tosti (1996). Individual measurements were binned with 12 hr bins.

(This table is available in its entirety in machine-readable form.)

The TESS observations are described in Kishore et al. (2024). The TESS filter covers the traditional Johnson I-band, but it is wider. Therefore, our first task is to connect the TESS magnitudes T with the Johnson I ones. We did it when OJ 287 was at a low level at the beginning of the TESS run at JD 2459500. At this time also the Swift telescope observed it as part of the MOMO project (Komossa et al. 2022). The spectral energy distribution is found to be quite normal, with the spectral index  $\alpha = -1.50 \pm 0.05$ . The R-T color is found to be 0.73, also as expected (Impey & Neugebauer 1988; Efimov et al. 2002; Kidger et al. 2018), if the TESS magnitude corresponds to the Johnson I-band magnitude. We assume in the following that this is the case. The TESS conversion formulae  $T = \log$  (counts  $s^{-1}$ ) + 20.44 and flux =  $6.064 \times 10^{-0.4(T-14)}$  mJy are used.  $^{26}$ 

The two light curves in the TESS and R-bands are similar in general. However, when we calculate the spectral index at

<sup>26</sup> https://tess.mit.edu/public/tesstransients/pages/readme.html

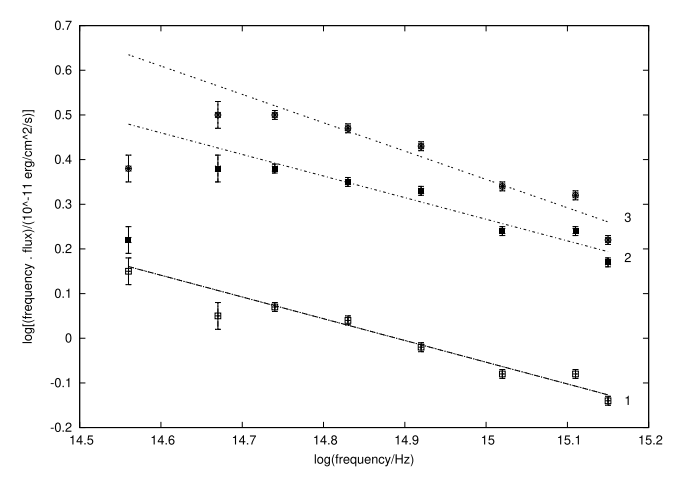


**Figure 4.** The spectral energy distribution in OJ 287 at the base level (1), at the light-curve hump (2), and in the early stages of the big flare (3).

different stages of the flare, differences arise. Figure 4 shows that during the flares (epochs 2 and 3), the spectral energy distribution peaks around the *R*-band frequency, in contrast to the base-level power-law spectrum where no such peak is seen (epoch 1). At the big flare, the spectral index at lower frequencies, between the *R* and *I* bands, is  $\alpha = -0.49 \pm 0.04$ , while in the background, it is  $\alpha = -1.50 \pm 0.05$ . Assuming that the base level stayed constant during the 9 day period between the beginning and the end of the flare period, the spectral index of the flare itself is  $\alpha \sim 0$ .

The spectral index differences show up also in colors. At the peak of the flare,  $R-T=0.165\pm0.008$ , while in the hump between JD 2459514 and JD 2459524, the spectrum flattens: at JD 2459519, we find  $R-T=0.105\pm0.03$ . The last Swift observation in this series was at JD 2459530, only 5 hr before the full peak of radiation, when we obtain  $R-T=0.11\pm0.06$ . The uncertainty in the R-band magnitude is large because the flux was rising fast and the nearest R-band measurement was done 2.5 hr later.

Kishore et al. (2024) estimate that the size of the emitting region is  $280 \pm 130$  au. Comparing this with the Schwarzschild radii of the two BHs in the model, 360 au and 3 au, respectively, we see that the emitting region must be located in the jet of the secondary BH, as jets widen considerably beyond the size of the BH of their origin (Gómez et al. 2022; Okino et al. 2022; Lu et al. 2023).

Another argument in support of the second component in the radiation during the flare is the behavior of the degree of polarization: while normally the degree of polarization increases with the rising flux (Gupta et al. 2023), in this instance it behaves quite the opposite way (Figure 2). This can be understood as superimposing two sources with different polarization properties in the same beam of light. Unfortunately, the polarization measurements did not cover the full radiation peak.

### 4. Probability of IDV

Even though the 2021 November 12 flare was the largest ever seen in the IDV timescale, the question remains: what is the likelihood that it simply represents the tail end in the IDV size distribution? For this purpose, we have sampled the *R*-band light curve from 2016 to 2023, which is dense enough for an IDV scale study and has only relatively small gaps during

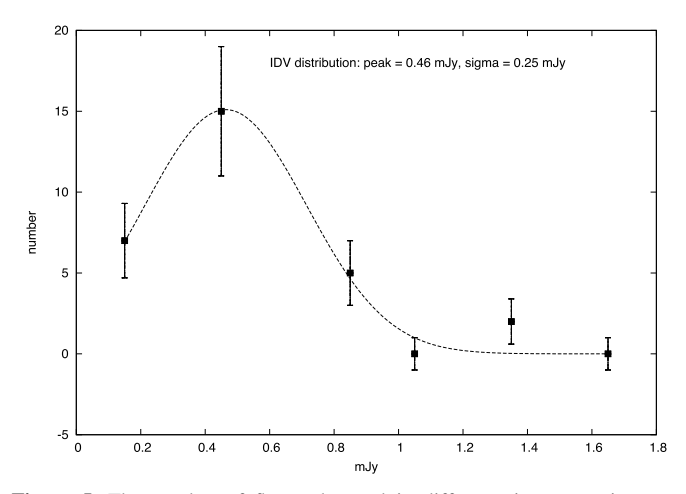


**Figure 5.** The number of flares observed in different size categories as a function of the mean flux density of the category. A Gaussian is fitted through the points. The 4.3 mJy flare is not shown.

the summer periods when OJ 287 is not visible from the ground. The FWHM of our 2021 November 12 flare is 0.5 day. Therefore, we chose to find and study all flares that satisfy the condition that their FWHM is not greater than 1 day, which is one way to define an IDV event.

The number distribution for the sample is shown in Figure 5. The 2021 November 12 flare is not included, as we want to consider it separately. There is a practical lower limit as to how small a variation is defined a flare. This causes a decline at the lower end of the distribution.

We fit a Gaussian to the distribution as shown in Figure 5. We see that our flare would be about nine standard deviations from the center of this distribution. The Gaussian tail may not be a good representation of the falloff of the numbers with size. If we use a power law, the numbers are expected to fall more slowly, but still we find that the 4.3 mJy flare is at least three standard deviations beyond what is expected. Thus, it is rather unlikely that our flare is just part of the normal variation in OJ 287. As long as we regard the normal variation as a property of the primary jet, the 2021 November 12 flare with its 4.3 mJy flux does not fit in the single-jet scenario.

#### 5. The Primary and the Secondary Jet

Radiation originating in the primary jet is seen from radio frequencies to X-rays, and the jet reaches into the megaparsec range (Marscher & Jorstad 2011). The jet is seen to wobble in a manner that can be explained by the influence of the secondary BH on the inner disk of the primary (Valtonen & Wiik 2012; Valtonen & Pihajoki 2013; Dey et al. 2021). The jet is thought to point almost directly toward us, which means that occasionally the jet passes through our line of sight. It causes in a big jump in the projected direction of the jet in the sky (Agudo et al. 2012; Dey et al. 2021). These jumps take place at different times at different frequencies, which is understandable if the jet is helical and radiation at different frequencies arises at different parts of the helix (Valtonen & Wiik 2012).

It has been suggested several times that the secondary BH also has a jet of its own (Villata et al. 1998; Pihajoki et al. 2013a, 2013b; Komossa et al. 2022). In the binary BH model, the spin of the primary is rather slow (Valtonen et al. 2016), and consequently, the jet is somewhat weak in relation to its mass. However, we have good reasons to expect that the

secondary BH spins near its maximum speed, and therefore its jet is quite bright. This high spin would be expected because the secondary receives and accretes a new dose of gas at every disk crossing, always with the same direction of the specific angular momentum.

Following Pihajoki et al. (2013b), we may estimate the number of orbital revolutions required to build the secondary spin up to its maximum value. According to simulations by Iwasawa et al. (2011), the number of close binary orbits leading to the present configuration of OJ 287 is of the order of 1 million. During each orbit, the secondary BH gains about 100  $M_{\odot}$  of rest mass. This is higher than the present rate since, in the standard magnetic accretion disk model, the accretion rate increases almost linearly with the impact distance and the orbit was typically an order of magnitude wider than it is today (Stella & Rosner 1984; Iwasawa et al. 2011). Therefore, in a million orbits, the rest mass of the secondary roughly doubles itself. This is enough to drive the spin value close to its maximum, even if started from zero (Bardeen 1970; Thorne 1974).

Ghosh & Abramowicz (1997) calculate the jet luminosity in the *Blandford–Znajek* process (Blandford & Znajek 1977) as follows:

$$L_j \sim m^{1.1} \dot{m}^{0.8} J^2,$$
 (1)

where m is the mass of the BH,  $\dot{m}$  is the mass accretion rate, and J is its normalized spin. For the primary, J=0.38 (Dey et al. 2018), and for the secondary,  $J\sim 1$ . In the normalization, we divide by m, which necessarily takes a J close to 1 or the maximum value, for small m. Using  $\dot{m}=1$  for the secondary (the Eddington rate) and  $\dot{m}=0.08$  for the primary (Valtonen et al. 2019) makes the secondary jet 43% of the total luminosity.

During the disk crossing, the secondary has the possibility of accreting large amounts of gas from the primary disk at a rapid rate, leading to a super-Eddington rate and a large increase in brightness. On the other hand, the impact on the disk tends to strip the secondary disk of its outer layers, and the disk-crossing-related events should be short-lived.

#### 6. Why Have We Not Seen Flares Like This Before?

We searched the optical light curve of OJ 287 during the OJ94 campaign, 1993–1998 (Pursimo et al. 2000); in the 2005–2010 campaign (Valtonen & Sillanpää 2011); and in the recent campaign (2015–2023, led by S.Z.; see machine-readable Tables 1 and 2), where very dense monitoring was carried out over the total period corresponding to approximately 10 yr worth of data. We found that there is only one flare that is even remotely similar to the 2021.86 flare in terms of amplitude (3.3 mJy in *R*) and rapidity (1 day): the 1993 December flare (Kidger et al. 1995).

According to Pihajoki et al. (2013b), a huge IDV flare should arise when the secondary BH meets dense clouds of gas during its 12 yr orbit. This happens most obviously at the disk crossing. Already before the crossing, the Roche lobe of the secondary is filled with dense gas. Some part of this gas falls inside the zone of 10 Schwarzschild radii from the secondary in a 0.08 yr timescale, and from there it is accreted to the secondary in about 0.02 yr. Thus, we expect to see the flare about 0.1 yr after the filling of the Roche lobe. The line in Figure 2 is copied from Pihajoki et al. (2013b), using the

Table 2
The Orbital Coordinates of the Secondary BH as well as V mag Observations of OJ 287 near the Dates of the Roche-lobe Flares and Impacts on the Disk

Date	X	Y	V mag	Event
(1)	(2)	(3)	(4)	(5)
1895.153	-16007.95	1144.43	•••	1895 flare
1895.444	-15361.20	147.85		1895 impac
1902.979	-17763.02	1500.39		1902 flare
1903.047	-17863.07	1309.48	14.90	Observation
1903.390	-18280.91	333.60		1903 impac
1912.442	-10862.75	680.36		1912 flare
1912.592	-11479.56	12.07		1912 impac
1923.627	-6306.61	370.52		1923 flare
1923.674	-6560.60	25.18	•••	1923 impac
1935.372	-4313.45	241.91	•••	1935 flare
1935.395	-4422.21	5.50	•••	1935 impac
1947.225	-3336.67	750.03	12.95	Observation
1947.270	-3494.69	208.14	≥13.70	1947 flare
1947.273	-3504.85	164.31	≥15.70	Observation
1947.285	-3536.00	18.59	14.00	1947 impact
1959.196	-3317.18	277.10	13.33	Observation
1959.201	-3319.03	208.64		1959 flare
1959.219	-3317.34	-19.38		1959 impact
1971.109	-3683.71	266.20		1971 flare
1971.129	-3628.91	18.16	13.07	1971 impac
1982.930	-4789.16	300.09		1982 flare
1982.960	-4653.19	3.87	14.363	1982 impac
1994.466	-7432.68	458.74		1994 flare
1994.537	-7104.67	-12.55		1994 impac
2004.949	-13271.67	1101.68	15.40	Observation
2004.957	-13251.91	1071.22		2004 flare
2004.963	-13236.68	1047.92	15.19	Observation
2005.166	-12676.68	250.00	14.40	2005 impact
2013.179	-17495.82	1357.36	14.82	Observation
2013.183	-17497.73	1346.63		2013 flare
2013.188	-17500.13	1333.22	14.91	Observation
2013.574	-17608.02	254.00		2013 impac
2021.859	-11805.82	704.78	15.21	Observation
2021.863	-11820.50	688.02	14.345	2021 flare
2021.872	-11850.30	654.00	15.29	Observation
2022.054	-12423.44	-47.73	14.85	2022 impac
2032.614	-6.610.41	402.34		2032 flare
2032.675	-6.905.54	2.61		2032 impac
2044.162	-4272.66	282.53		2044 flare
2044.192	-4411.38	-3.67		2044 impact

**Note.** The entire data set of coordinates, magnitudes, and upper brightness limits from 1887 to 2045 is available. Column 1: date. Columns 2 and 3: *X*- and *Y*-coordinates of the secondary BH. Column 4: *V*-band magnitude. Column 5: type of event. In each impact-related group, the date of the expected Rochelobe flare and its magnitude are given, in case observations were recorded on that night. The adjacent dates refer to the nearest observations, if any. The last line is for the date of impact of the secondary BH on the midplane of the disk.

(This table is available in its entirety in machine-readable form.)

assumption that the mass influx is directly proportional to brightness. No detailed model for the sharp flare is available from simulations.

In order to see where this places the OJ 287 flare in 2021, we have to look at the orbit dynamics at that time. Table 2 gives orbital phases as well as observed magnitudes during certain interesting times. It is an extract from a larger orbit-linked historical light curve of OJ 287 that is found in machine-readable full Table 2. The linking to the orbit is also done in the upper scale of Figure 2, which tells the position of the secondary above the disk.

From machine-readable full Table 2, we may read that the secondary is 1150 au above the midplane of the disk at 2021.756. The significance of this level above the midplane is that it has the value of the Roche-lobe radius of the secondary (Eggleton 1983); i.e., just at this time, the secondary BH has started to swallow the gas of the primary disk. The sharp flare is observed at 2021.863. This is  $\sim$ 0.1 yr later, as was estimated by Pihajoki et al. (2013b). As they pointed out, the final accretion spike arises in only a few orbital times. If we take the period of the innermost stable orbit, estimated to be 3.8 hr (Pihajoki et al. 2013a), as the reference number, we find a good agreement with the 12 hr observed spike.

Note that the time of the Roche-lobe flare is theoretically specified within an interval of  $\pm 0.01$  yr. The accidental chance of detecting an exceptional flare at this time is less than 0.2%, since the probability of finding such a flare in the 10 yr of monitoring data is less than unity.

As Figure 3 illustrates, these events are only visible to us when the secondary hits the disk from above, as seen from our direction. Thus, there is an opportunity to see a flare like this only once in 12 yr. And to meet the opportunity, an observer has to take measurements not only on a correct night but also in the correct few-hour interval during that night. We would have also missed this flare this time if we did not have a warning that something interesting might happen in this time frame, which alerted observers to do their best for a fast sampling of the light curve.

In order to calculate the predicted flare time at other instances, we may simply scale the Roche-lobe filling level above the disk with the distance from the primary BH. This is because the radius of the Roche lobe scales with this distance. Also, the relevant astrophysical speeds scale with the distance from the center of the accretion disk, basically due to Kepler's second law. Thus, we may take the level of the secondary above the disk at the spike (see the upper scale in Figure 2) and use it as a reference number, which is then scaled linearly to other impact distances. The timing is then calculated using machine-readable full Table 2. The results are shown in Table 2.

We find that in the past there has only been one observation on the night in question. This happened in 1947 when a photographic plate was taken at Sonneberg Observatory in Germany, including the position of OJ 287 in the sky, at the right time on JD 2432287, obviously for other purposes. One of us (R.H.) has confirmed that the detection limit on this plate was rather poor, and one cannot see anything at the position of OJ 287. Thus, the detection would not have been possible.

#### 7. Conclusions

The 2021/22 observing campaign of OJ 287 was planned in anticipation of a major cosmic crash: a  $1.5 \times 10^8~M_\odot$  BH crashing through the accretion disk of another, bigger BH. The epoch of this event was uncertain by some months since the position of the disk in the system was not yet known. It was calculated only later. Even though such events are thought to arise regularly in OJ 287, never before had an extensive campaign been directly aimed at this particular epoch. Previously, the observations were concentrated on signals that arise from the material expelled from the disk. Since such major signals were expected in 2022 July/August, when the source is unobservable from the ground, the emphasis this time was on the direct signals from the impact.

What was expected, and had been discussed already several years earlier by Pihajoki et al. (2013b), was the temporary activation of the jet from the  $1.5 \times 10^8~M_\odot$  BH. Since the secondary BH is 122 times smaller than the primary in the solution by Dey et al. (2018), the timescales associated with the secondary jet should be correspondingly shorter. Therefore, we had to look for IDV events. Purely from energetic grounds, it is unlikely that the primary jet could be operated by a sufficiently small BH that it could produce major flares in the IDV timescale (Valtonen et al. 2023d).

The 2021 November 12 (at 2 a.m. UT) flare was fortunately well covered by the TESS campaign (Kishore et al. 2024) in the *I* band (or close to it) and our campaign in the *R*-band. Both observed an increase of the flux by more than a magnitude in a few days, and the rise of the last half of the flare took place in only a quarter of a day. The observations allow us to compare the *R*-*I* spectral index in and out of the flare. The difference is clear: the spectrum is flatter in the flare with respect to the background by  $\Delta \alpha \sim 1.0 \pm 0.1$ . If we consider the likely separation of the base and the flare components, the difference is even clearer,  $\Delta \alpha = 1.5 \pm 0.1$ .

The large change of the spectral index around the *R*-band frequency is difficult to understand purely as aging of the population of relativistic electrons (Pacholczyk 1970; Impey & Neugebauer 1988). The situation resembles the spectral behavior normally seen at the radio frequencies (Marscher & Gear 1985). The flat-spectrum turnover frequency would then be  $\sim 10^3$  times higher than what is typically observed in quasars (Valtaoja et al. 1992). This could result from a different magnetic flux density and/or size of the emitting region in the secondary jet than in the primary jet.

The secondary jet origin of the radiation at this time is also deduced from the behavior of polarization, even though the coverage is not as complete as the spectral index coverage. The variability timescale puts strict limits on the size of the emission region in the IDV flare and places it most likely inside the jet of the smaller BH.

The short life of the IDV flare, only 12 hr above the half-maximum value, makes it very difficult to detect by a single telescope on the ground. It may happen during the daytime or a cloudy period at that telescope site. Or it may just happen that there is a break in the observing schedule for some reason. Thus, the Skynet Robotic Telescope Network, with telescopes on four continents, as well as the dedicated TESS satellite monitoring, were crucial to this discovery.

There are previous examples in the monitoring of OJ 287 flares where the peak activity was missed for various technical reasons (e.g., the peak of the 1995 major flare and the polarization measurement of the peak of the 2005 major flare). Therefore, we were fortunate this time even if we knew reasonably well what to look for and when.

The detection of the 2021 November 12 flare may also be viewed as an additional confirmation of the Dey et al. (2018) orbit solution. Since we are lacking a detailed theory of the secondary BH jet activation process, we could not predict to the day when the IDV flare should have happened. However, now that we have seen one such case, we can reasonably calculate when such events should have happened in the past. It seems that we have missed them all. Also, we can give fair estimates of when they will happen again: in 2033 August and 2044 March. The former event requires space-based observations, but fortunately there is plenty of time to prepare for them.

#### Acknowledgments

This study was based in part on observations conducted using the Perkins Telescope Observatory (PTO) in Arizona, USA, which is owned and operated by Boston University. The research at Boston University was supported in part by National Science Foundation grant AST-2108622 and a number of NASA Fermi Guest Investigator grants; the latest is 80NSSC23K1507. This work was partly funded by NCN grant No. 2018/29/B/ST9/01793 (S.Z.) and JSPS KAKENHI grant No. 19K03930 (K.M.). S.C. acknowledges support by ASI through contract ASI-INFN 2021-43-HH.0 for SSDC and the Instituto Nazionale di Fisica Nucleare (INFN). R.H. acknowledges the EU project H2020 AHEAD2020, grant agreement 871158, and internal CTU grant SGS21/120/ OHK3/2T/13. A.C.G. is partially supported by the Chinese Academy of Sciences (CAS) President's International Fellowship Initiative (PIFI; grant No. 2016VMB073). M.F.G. is supported by the National Science Foundation of China (grant 11873073), the Shanghai Pilot Program for Basic Research-Chinese Academy of Science, Shanghai Branch (JCYJ-SHFY-2021-013), the National SKA Program of China (grant No. 2022SKA0120102), the science research grants from the China Manned Space Project with No. CMSCSST-2021-A06, and the Original Innovation Program of the Chinese Academy of Sciences (E085021002). Z.Z. is thankful for support from the National Natural Science Foundation of China (grant No. 12233005). The work is partly based on observations made with the Nordic Optical Telescope, owned in collaboration by the University of Turku and Aarhus University and operated jointly by Aarhus University, the University of Turku, and the University of Oslo, representing Denmark, Finland, and Norway and the University of Iceland and Stockholm University at the Observatorio del Roque de los Muchachos, La Palma, Spain, of the Instituto de Astrofisica de Canarias. This study is based in part on observations obtained with telescopes of the University Observatory Jena, which is operated by the Astrophysical Institute of the Friedrich-Schiller University. M.J.V. acknowledges a grant from the Finnish Society for Sciences and Letters.

## **ORCID iDs**

```
Mauri J. Valtonen https://orcid.org/0000-0001-8580-8874
Staszek Zola https://orcid.org/0000-0003-3609-382X
Alok C. Gupta https://orcid.org/0000-0002-9331-4388
Shubham Kishore https://orcid.org/0000-0001-8716-9412
Svetlana G. Jorstad https://orcid.org/0000-0001-6158-1708
Paul J. Wiita https://orcid.org/0000-0002-1029-3746
Minfeng Gu https://orcid.org/0000-0002-4455-6946
Kari Nilsson https://orcid.org/0000-0002-1445-8683
Alan P. Marscher https://orcid.org/0000-0001-7396-3332
Zhongli Zhang https://orcid.org/0000-0002-8366-3373
Katsura Matsumoto https://orcid.org/0000-0002-
5277-568X
Andrei V. Berdyugin https://orcid.org/0000-0002-
9353-5164
Daniel E. Reichart https://orcid.org/0000-0002-5060-3673
Markus Mugrauer https://orcid.org/0009-0002-2791-1341
Lankeswar Dey https://orcid.org/0000-0002-2554-0674
Tapio Pursimo https://orcid.org/0000-0002-5578-9219
Stefano Ciprini https://orcid.org/0000-0002-0712-2479
M. Uemura https://orcid.org/0000-0002-7375-7405
```

```
Ryo Imazawa https://orcid.org/0000-0002-0643-7946 Michal Zejmo https://orcid.org/0000-0001-5836-9503 Vladimir V. Kouprianov https://orcid.org/0000-0003-3642-5484 James W. Davidson, Jr. https://orcid.org/0009-0007-1284-7240 Alberto Sadun https://orcid.org/0000-0001-8086-7242 Z. R. Weaver https://orcid.org/0000-0001-6314-0690
```

#### References

```
Agudo, I., Marscher, A. P., Jorstad, S. G., et al. 2012, ApJ, 747, 63
Bardeen, J. M. 1970, Natur, 226, 64
Blandford, R. D., & Znajek, R. L. 1977, MNRAS, 179, 433
Dey, L., Valtonen, M. J., Gopakumar, A., et al. 2018, ApJ, 866, 11
Dey, L., Valtonen, M. J., Gopakumar, A., et al. 2021, MNRAS, 503, 4400
Efimov, Y. S., Shakhovskoy, N. M., Takalo, L. O., & Sillanpää, A. 2002,
   A&A, 381, 408
Eggleton, P. P. 1983, ApJ, 268, 368
Fiorucci, M., & Tosti, G. 1996, A&AS, 116, 403
Ghosh, P., & Abramowicz, M. A. 1997, MNRAS, 292, 887
Gupta, A. C., Kushwaha, P., Valtonen, M. J., et al. 2023, ApJL, 957, 11
Gómez, J. L., Traianou, E., Krichbaum, T. P., et al. 2022, ApJ, 924, 122
Impey, C. D., & Neugebauer, G. 1988, AJ, 95, 307
Ivanov, P. B., Igumenshchev, I. V., & Novikov, I. D. 1998, ApJ, 507, 131
Iwasawa, M., An, S., Matsubayashi, T., Funato, Y., & Makino, J. 2011, ApJL,
Kidger, M., Zola, S., Valtonen, M., et al. 2018, A&A, 610, A74
Kidger, M. R., Gonzalez-Perez, J. N., de Diego, J. A., et al. 1995, A&AS,
Kishore, S., Gupta, A. C., & Wiita, P. J. 2024, ApJ, 960, 11
Komossa, S., Grupe, D., Kraus, A., et al. 2022, MNRAS, 513, 3165
Laine, S., Dey, L., Valtonen, M., et al. 2020, ApJL, 894, L1
Lehto, H. J., & Valtonen, M. J. 1996, ApJ, 460, 207
Lu, R.-S., Asada, K., Krichbaum, T. P., et al. 2023, Natur, 616, 686
Marscher, A. P., & Gear, W. K. 1985, ApJ, 298, 114
Marscher, A. P., & Jorstad, S. G. 2011, ApJ, 729, 26
Mikkola, S. 2020, Gravitational Few-body Dynamics: A Numerical Approach
   (Cambridge: Cambridge Univ. Press)
Miller, R. H. 1976, JCoPh, 21, 400
Okino, H., Akiyama, K., Asada, K., et al. 2022, ApJ, 940, 17
Pacholczyk, A. G. 1970, Radio Astrophysics. Nonthermal Processes in
   Galactic and Extragalactic Sources (San Francisco, CA: Freeman)
Pihajoki, P., Valtonen, M., & Ciprini, S. 2013a, MNRAS, 434, 3122
Pihajoki, P., Valtonen, M., Zola, S., et al. 2013b, ApJ, 764, 5
Pursimo, T., Takalo, L. O., Sillanpaa, A., et al. 2000, A&AS, 146, 141
Salo, H. 2012, PThPS, 195, 48
Sillanpaa, A., Haarala, S., Valtonen, M. J., Sundelius, B., & Byrd, G. G. 1988,
   ApJ, 325, 628
Sitko, M. L., & Junkkarinen, V. T. 1985, PASP, 97, 1158
Stella, L., & Rosner, R. 1984, ApJ, 277, 312
Sundelius, B., Wahde, M., Lehto, H. J., & Valtonen, M. J. 1997, ApJ, 484, 180
Thorne, K. S. 1974, ApJ, 191, 507
Valtaoja, E., Terasranta, H., Urpo, S., et al. 1992, A&A, 254, 71
Valtonen, M., & Pihajoki, P. 2013, A&A, 557, A28
Valtonen, M., & Sillanpää, A. 2011, AcPol, 51, 76
Valtonen, M., Zola, S., & Gopakumar, A. 2023a, BAAS, 55, 2023n6i322p03
Valtonen, M. J. 2007, ApJ, 659, 1074
Valtonen, M. J., Dey, L., Gopakumar, A., et al. 2021, Galax, 10, 1
Valtonen, M. J., Dey, L., Gopakumar, A., et al. 2023b, Galax, 11, 82
Valtonen, M. J., Lehto, H. J., Nilsson, K., et al. 2008, Natur, 452, 851
Valtonen, M. J., Mikkola, S., Lehto, H. J., et al. 2011, ApJ, 742, 22
Valtonen, M. J., & Wiik, K. 2012, MNRAS, 421, 1861
Valtonen, M. J., Zola, S., Ciprini, S., et al. 2016, ApJL, 819, L37
Valtonen, M. J., Zola, S., Gopakumar, A., et al. 2023c, MNRAS, 521, 6143
Valtonen, M. J., Zola, S., Gopakumar, A., et al. 2023d, MNRAS, 525, 1153
Valtonen, M. J., Zola, S., Pihajoki, P., et al. 2019, ApJ, 882, 88
Villata, M., Raiteri, C. M., Sillanpaa, A., & Takalo, L. O. 1998, MNRAS,
  293, L13
Zola, S., Kouprianov, V. V., Reichart, D. E., Bhatta, G., & Caton, D. B. 2021,
    MxAC, 53, 206
Zwick, L., & Mayer, L. 2023, MNRAS, 526, 2754
```